ADVANCED OPTICAL MATERIALS
www.advopticalmat.de

Wide-Field Optical Microscopy of Microwave Fields Using Nitrogen-Vacancy Centers in Diamonds

*Linbo Shao, Ruishan Liu, Mian Zhang, Anna V. Shneidman, Xavier Audier, Matthew Markham, Harpreet Dhillon, Daniel J. Twitchen, Yun-Feng Xiao, and Marko Lončar**

Spatial and spectral analysis of electromagnetic fields[1] at microwave frequencies is crucial for many applications, spanning a wide range of disciplines. Examples include the study of quantum electromagnetic metamaterials,[2,3] nanomaterials,[4] magnonics,[5–7] integrated circuit analysis,[8] and biological sensing.[9] In the past decades, scanning probe microscopy,[10–12] superconducting quantum interference devices,[13,14] and atomic vapor cells[15,16] have been used to improve the sensitivity and frequency resolution of microwave microscopy. However, the requirements of a scanning mechanism, cryogenic cooling, and/or a relatively large sensor size limit their relevance for practical applications.

Here we demonstrate wide-field optical microscopy of microwave fields using ensembles of nitrogen-vacancy (NV) color centers in diamond. Owing to NV properties, the microwave field can be mapped onto the population of spin states of NV centers, which in turn can be read out optically.[17] The negatively charged NV center is a lattice defect in diamond, which consists of a substitutional nitrogen atom and an adjacent vacancy. The spin states of NV centers can be optically addressed and are sensitive to DC and AC magnetic fields.[18,19] To date, NV centers have been utilized in magnetometry,[20–23] nuclear magnetic resonance detection,[24–30] targeted cells imaging,[31] and intracell thermometry.[32] Recently, the ability of NV centers to detect microwave magnetic fields has also been investigated.[33–38] Pulsed laser sequences[33–37] were used to measure Rabi oscillations between different spin ground states, and scanning probe techniques[37] were used to achieve nanoscale resolution. For many practical applications, however, wide field imaging and a simple experimental procedure are beneficial. To accomplish this, we opt for continuous wave laser excitation[35,38] to measure the spin populations of NVs in the presence of microwave fields using a conventional inverted microscope. In this way, we demonstrate wide-field imaging of microwave fields over a 200 × 200 μm^2 area with submicrometer spatial resolution, and spectral analysis of the microwave field with a resolution bandwidth of 460 kHz (i.e., the linewidth of NV). Minimum detectable microwave power of tens of nanowatts and a large dynamic range of over 33 dB in microwave power is obtained. Importantly, by using a bias magnetic field we could control the microwave frequency that NV centers are sensitive to—via Zeeman effect—over a frequency range of 170 MHz (potentially up to 100 GHz (ref. [35])). In addition, we demonstrate a high frequency sensitivity of 2.5 kHz Hz$^{-1/2}$ for a single frequency-modulated microwave signal detection.

A schematic of our apparatus is depicted in **Figure 1**a (see Figure S1 in the Supporting Information for the detailed experimental setup). A diamond chip containing a thin layer of NV centers with NV density of 3–4 ppm and linewidth of 460 kHz (see the Experimental Section for detail) contributes to spatial and spectral resolutions and signal-to-noise ratio. This diamond chip is closely placed on top of a microwave circuit under investigation, allowing near field imaging of microwave fields. An inverted optical microscope is used to deliver green (532nm) laser probe light and NV fluorescence (600–750 nm) is collected through the same objective. The collected light is filtered and focused onto an electron-multiplying charge coupled device (EM-CCD) for imaging. An electromagnet is used to provide a bias DC magnetic field B_0 that controls the frequency splitting ν_0 between the NV's spin 0 ground state $|0\rangle_g$ and the spin −1 ground state $|-1\rangle_g$, according to $\nu_0 = D_0 - \gamma B_0$. Here, $D_0 = 2.87\,\mathrm{GHz}$ is the crystal field splitting and $\gamma(2\pi) = 28\,\mathrm{MHz\,mT^{-1}}$ is the gyromagnetic ratio. For simplicity, in this work we align B_0 with one of possible NV orientations and focus on states $|-1\rangle_g$ and $|0\rangle_g$, only. The spectral analysis of an unknown microwave field is accomplished by scanning ν_0 over a wide frequency range, by sweeping a voltage applied to the electromagnet, while monitoring the NV fluorescence intensity. As illustrated in Figure 1b, when the microwave frequency f_{RF} is resonant with ν_0, the NV is driven from $|0\rangle_g$ to $|-1\rangle_g$ by the microwave magnetic field with polarization perpendicular

L. Shao, R. Liu, Dr. M. Zhang, A. V. Shneidman, X. Audier, Prof. M. Lončar
John A. Paulson School of Engineering and Applied Science
Harvard University
29 Oxford Street, Cambridge, MA 02138, USA
E-mail: loncar@seas.harvard.edu
R. Liu, Prof. Y.-F. Xiao
State Key Laboratory for Mesoscopic Physics and School of Physics
Peking University
5 Yiheyuan Road, Beijing 100871, China
A. V. Shneidman
Department of Chemistry and Chemical Biology
Harvard University
12 Oxford Street, Cambridge, MA 02138, USA
Dr. M. Markham, H. Dhillon, Dr. D. J. Twitchen
Element 6, Element Six Innovation, Fermi Avenue
Harwell Oxford
Didcot, Oxfordshire OX110QR, UK

DOI: 10.1002/adom.201600039

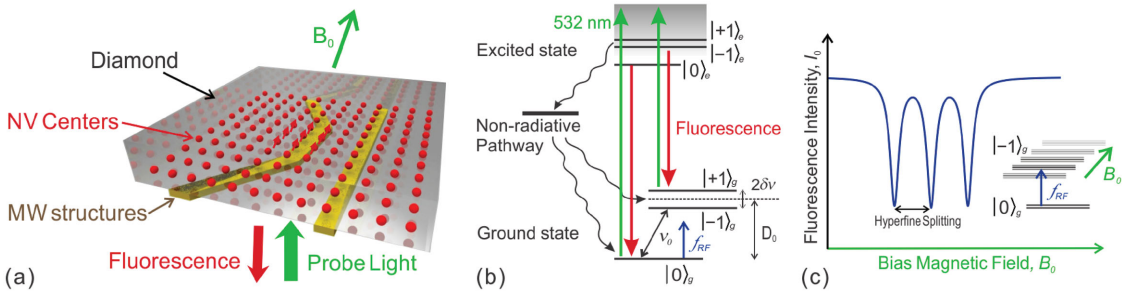

Figure 1. Experimental configuration and principle of optical microscopy and spectroscopy of microwave field using NV centers in diamond. a) Schematic of the experimental setup. b) Simplified electronic energy levels of negatively-charged NV center. The ground state is a spin triplet with a splitting ν_0 between the spin-0 ground state $|0\rangle_g$ and the spin-(–1) ground state $|\pm1\rangle_g$ determined by crystal field splitting D_0, and Zeeman shift $\delta\nu$ induced by an external magnetic field B_0, which is aligned with the orientation of one class of NV centers. The nonradiative pathway (wiggly arrows) enables optical polarization and readout of the NV spin states. c) A frequency spectrum of a single frequency microwave signal obtained by scanning the external magnetic field B_0. When a microwave signal is on resonance with the splitting between $|0\rangle_g$ and $|-1\rangle_g$, three dips in fluorescence intensity will be observed due to hyperfine interactions with the ^{14}N atom of NV center.

to the NV axis.[34] This results in a reduction in the fluorescence intensity, since $|-1\rangle_e$ has a higher nonradiative decay rate than $|0\rangle_e$.[39–41] Therefore, the amplitude of microwave magnetic fields can be determined by measuring the fluorescence contrast with and without microwave signals. Each frequency in the microwave signal results in three dips in NV fluorescence intensity as a result of hyperfine interactions with the nuclear spin of the ^{14}N in the NV center[39] (Figure 1c).

To characterize the efficacy of NV centers as microwave spectrum analyzers, the fluorescence is measured (averaging over a 5 × 5 μm^2 region at the central field of view) in the presence of known microwave signals with various frequencies and intensities. First, the apparatus is calibrated by detecting harmonic microwave signals of known frequency (in the range of 2.72 to 2.84 GHz) (**Figure 2**a). The calibration curve, shown in Figure 2b, features the linear dependence of ν_0 on the voltage supplied to the electromagnet, with the slope $S = -18.12(6)$ MHz V^{-1}. From the fit, we also obtain the zero field splitting value $D_0 = 2.866\,6(3)$ GHz which is in perfect agreement with the literature value reported at room temperature.[42] With this calibration, we obtain the spectra (blue lines in Figure 2c) of more complex microwave signals, and compared the results with the spectra (red lines) obtained using a real-time spectrum analyzer (RSA). Good agreement between two sets of data is observed. The small discrepancy in the absolute spectral line position can be attributed to mechanical instability of the setup and hysteresis of the electromagnet.

Next, we demonstrate that NV centers can be used as a tunable microwave spectrum analyzer, whose sensitivity level and dynamic range can be adjusted by the probe laser power. As shown in Figure 2d, adjusting the laser power from 28 μW to 33 mW allows detection of microwave signals with powers in the range of –50 dBm to –10 dBm measured at the output of function generator. (The microwave frequency f_{MW} is fixed at 2.834 GHz for this measurement. A detailed study of the dependence of the fluorescent contrast on microwave and laser powers is summarized in Figure S3 in the Supporting Information.) A logarithmic dependence of fluorescence contrast on the microwave power and a dynamic range of 33 dB of microwave power (from –45 dBm to –12 dBm) are achieved by an intermediate probe laser power of 1.49 mW (black line in Figure 2d) measured at the input port of microscope. We thus estimate the amplitude sensitivity of our apparatus to be ≈45 nT Hz$^{-1/2}$ (See Note I of the Supporting Information) for the 5 × 5 μm^2 region. At a higher laser power of 33.86 mW (red line), the fluorescence contrast linearly depends on the microwave magnetic field amplitude as shown in Figure 2d inset.

We image microwave fields by simultaneously measuring the fluorescence of NV center ensembles at all positions in the field of view of the microscope. The microwave structure (**Figure 3**a) consists of two 20 μm wide gold transmission lines realized on microscope coverslip, using standard microfabrication techniques. The gap between the two lines varies from 20 to 40 μm across the field of view. In this demonstration, the transmission line on the right (left) carries a –10 dBm microwave signal of radio frequency RF_1 = 2.78 GHz (RF_2 = 2.80 GHz). The fluorescence contrasts indicating the microwave field amplitude are measured by tuning NV centers in resonance with RF_1 and RF_2 are shown in Figure 3b,c, respectively. The spectra of microwave fields at three positions indicated in Figure 3a are shown in Figure 3d–f. In these figures, the depths of resonance dips represent the amplitudes of microwave field: the larger the amplitude, the larger the dip. As expected, while the amplitude of the microwave field is almost identical in the gap between the two transmission lines, there are significant differences on either side of the transmission lines. Cross-talk between two lines is also observed, as expected, since the wavelength of the microwave (10.7 cm) signal used is much larger than the feature sizes of the circuit.

Owing to the narrow linewidth of its hyperfine lines, the NV center can effectively transduce small variations in the frequency of microwave signals to measurable changes in the fluorescence intensity. Thus, NV centers are promising candidates for low-noise frequency modulation spectroscopy.[43] In this work, we demonstrate the ability of NV centers to detect frequency-modulated (FM) microwave signals in real time using the same experimental apparatus. In general, an FM signal can be written as $y(t) = A_c \cos(2\pi(f_c + k_{FM}x(t))t)$, where A_c is the amplitude of microwave carrier signal, f_c is the carrier frequency, and k_{FM} is the amplitude-to-frequency gain. $x(t)$ is a modulating signal, which, in its simplest form, can be written as $x(t) = A_m \cos(2\pi f_m t)$. A_m and f_m are amplitude and

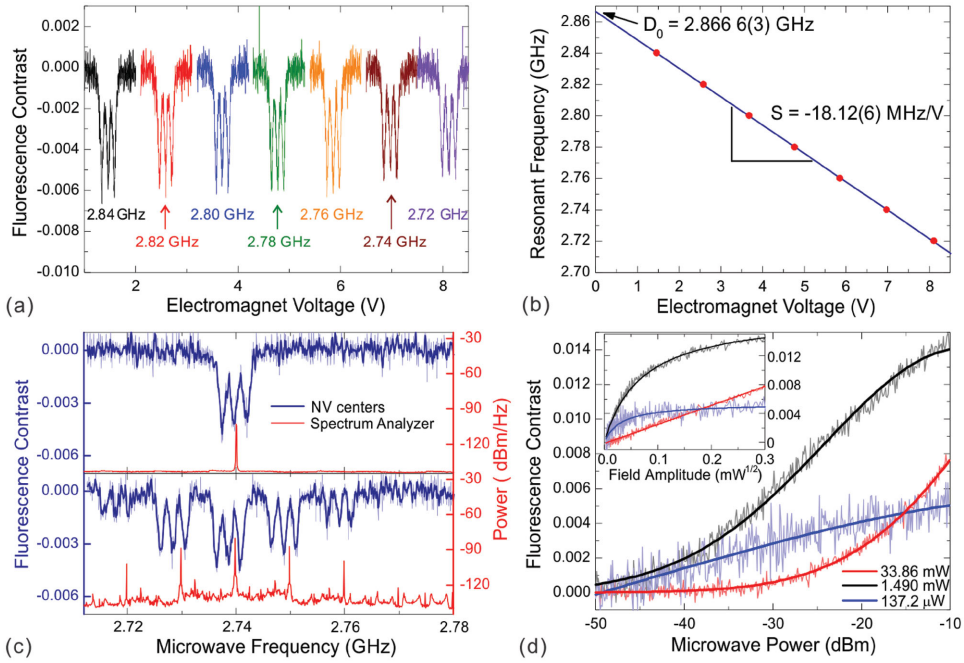

Figure 2. Microwave spectroscopy using NV centers. a) Fluorescence contrast of NV centers as a function of voltages driving the electromagnet, in the presence of microwave signals having frequencies from 2.72 GHz to 2.84 GHz. This data set is used to calibrate the apparatus and b) to establish the relationship between the applied voltage and NV resonant frequencies. Each point in (b) is extracted by fitting measurements in (a) to three Lorentzians. The magnitudes of fitting error is less than 0.7 mV (smaller than the size of data points, see detail in Figure S2 in the Supporting Information). c) Microwave spectra acquired using NV centers (blue lines) and a real-time spectrum analyzer (RSA, red lines). In the upper panel, a simple harmonic microwave signal with frequency of 2.74 GHz was used, while in the lower one signal centered at 2.74 GHz with side bands separated by 10 MHz was used. The single-pass scanning data obtained by taking one EM-CCD frame at each frequency are shown in light blue, while three frames shift-averaged data are shown in dark blue. The resolution bandwidth of the RSA is 20 kHz. d) The fluorescence contrast of NV centers exposed to microwave powers from –50 to –10 dBm and probe laser powers of 137.2 μW (blue lines), 1.49 mW (black lines), and 33.86 mW (red lines). The thin lines in light colors are the measurement data, while the thick lines are the fitted curves. The microwave frequency is fixed at 2.834 GHz. Inset: same data with x-axis proportional to the amplitude of magnetic field component of the microwave signal. The fluorescence data in this figure are averaged over a 5×5 μm^2 region near the central field of view.

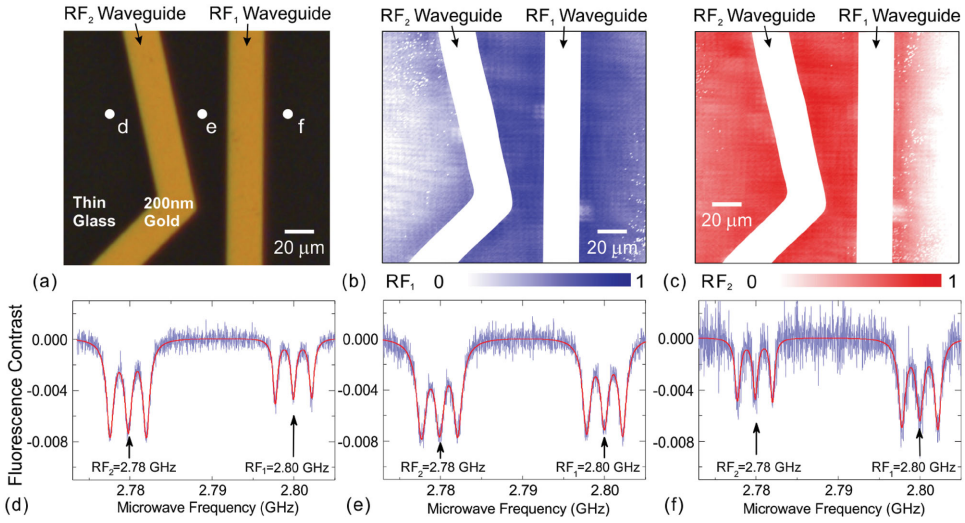

Figure 3. Imaging the microwave field. a) A microscope image of the microwave structure with two gold transmission lines fabricated on a cover glass. The left and right line carries microwave signal at radio frequency RF_1 and RF_2, respectively. b,c) The images of fluorescence contrast of NV centers at frequency b) $RF_1 = 2.80$ GHz and c) $RF_2 = 2.78$ GHz. The RF intensity scale bars are in arbitrary unit. d–f) The microwave spectra from three positions indicated in (a). The powers of the microwave signal are –10 dBm.

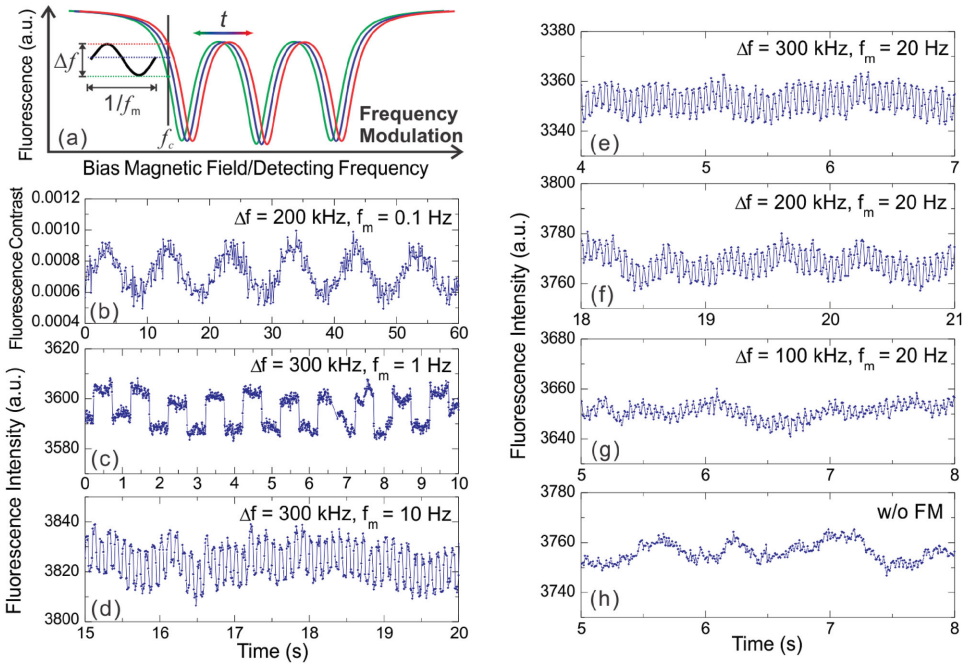

Figure 4. Real-time detection of frequency modulated microwave signals. a) Principle of frequency modulation (FM) detection. A constant bias magnetic field fixes the detecting microwave frequency at the position of maximum slope. Thus frequency changes of the microwave signal induce fluctuations of NV fluorescence. Δf indicates the maximum frequency deviation of microwave signal from carrier frequency f_c, and f_m represents the frequency of modulating signal. The spectra in different colors indicate the signal at different times t. b) Fluorescence contrast of NV centers for a microwave signal frequency-modulated by an $f_m^{-1} = 10$ s sine wave. The capture rate is about 14 frames per second. c–g) Real-time fluorescence intensity of NV centers in response to microwave signals frequency-modulated by square waves. The frequency deviation Δf is changed from 300 to 100 kHz, while the modulating frequency f_m is changed from 1 to 20 Hz. The capture rate is about 112 frames per second. h) Real-time fluctuations of fluorescence intensity without modulating signal present.

frequency of the modulating signal, respectively. Therefore, the time-dependent frequency of the FM microwave signal can be written as $f(t) = f_c + \Delta f \cos(2\pi f_m t)$, where $\Delta f = k_{\mathrm{FM}} A_m$ is the maximum frequency deviation.

The principle of NV-based FM detection is depicted in **Figure 4**a. To achieve the best performance, the operating point is chosen by selecting the value of B_0 so that the FM carrier frequency f_c corresponds to the position of maximum slope on the curve, indicated by the black vertical lines in Figure 4a. The time-dependent frequency component $\Delta f \cos(2\pi f_m t)$ of the microwave signal is then mapped to the fluctuation of fluorescence intensity. This fluctuation is finally recorded by the EM-CCD, and the original signal $x(t)$ is recovered.

We detected frequency-modulated microwave signals with various frequency deviations Δf and modulating frequencies f_m. Figure 4b shows the results for a sine-wave with $\Delta f = 200$ kHz and $f_m = 0.1$ Hz. For this low frequency measurement, we take reference frames and detection frames alternatively (with same exposure time) to cancel out low frequency ($1/f$) noise, and obtain a sensitivity of 4 kHz $\mathrm{Hz}^{-1/2}$ at $f_m = 0.1$ Hz (Figure S4a, Supporting Information). Figure 4 c–g show demodulated FM microwave signals when the signal $x(t)$ is a square wave with $f_m = 1$ Hz and $f_m = 20$ Hz, and Δf varies from 100 to 300 kHz. The demodulated signals resemble the original modulating signals with the same frequency f_m as $x(t)$, and the amplitude of the demodulated signal is proportional to Δf. The measurement of fluorescence fluctuations without FM is plotted in Figure 4h.

The fluorescence contrast is an important figure of merit that determines the sensitivity and dynamic range for microwave field detection. As shown in Figure 2d, and discussed in detail in the Supporting Information, the fluorescence contrast is strongly dependent on the microwave and laser power used. In our experiments, the NV is continuously driven into the $|0\rangle_g$ state with an effective optical polarization rate G_{op}, determined by the power of the probe laser, while the applied microwave field drives the NV centers from $|0\rangle_g$ to $|-1\rangle_g$ with a Rabi frequency Ω_{MW}. The steady fluorescence contrast C at resonance is given by

$$C = \frac{(1-\beta)\xi G_{\mathrm{OP}}}{(1+\beta)\gamma_1 + G_{\mathrm{OP}}} \times \frac{2\Omega_{\mathrm{MW}}^2}{4\Omega_{\mathrm{MW}}^2 + \gamma_2(2\gamma_1 + G_{\mathrm{OP}})} \quad (1)$$

where $\xi = 1/12$ is the portion of NVs on resonance with the applied microwave signal (due to other NV directions and nuclear spin states), β is the ratio of fluorescence intensity of $|-1\rangle_g$ to $|0\rangle_g$, γ_1 is relaxation rate of ground state due to spin-lattice relaxation, γ_2 is dephasing rate of the ground state, all these parameters are material properties (i.e., not dependent on the laser power or microwave field amplitude). When the amplitude of microwave field is small $(\Omega_{\mathrm{MW}}^2 \ll \gamma_2(2\gamma_1 + G_{\mathrm{OP}}))$, the contrast $C \propto \Omega_{\mathrm{MW}}^2 / G_{\mathrm{OP}}$ assuming $G_{\mathrm{OP}} \gg \gamma_1$, which indicates a lower laser power should be used to measure a week microwave field. However, for a strong microwave field $(\Omega_{\mathrm{MW}}^2 \gg \gamma_2(2\gamma_1 + G_{\mathrm{OP}}))$,

the contrast C will saturate to a constant, where G_{OP} determines the saturation amplitude of the microwave field. In other words, greater G_{OP} results in a larger dynamic range of microwave amplitude measurements. This dependency of the contrast given by Equation (1) is plotted Figure S9 (Supporting Information), which is in agreement with the experimental data shown in Figure 4d and Figure S3 (Supporting Information). Since some parameters in Equation (1) might be challenging to be experimentally measured, the dependence of contrast C on microwave amplitude could also be calibrated by measuring Rabi frequencies[34,37] when detection of absolute amplitude of microwave magnetic field is preferred.

For spectroscopic measurements, the linewidth of microwave transition determines the resolution bandwidth of the NV centers as a spectrum analyzer (see Notes 2–4 in the Supporting Information). The linewidth of the hyperfine line is measured about 460 kHz for the diamond sample (see Figure S7 in the Supporting Information). It could be affected by dipolar coupling to other nuclear spins near the system, such as neighboring ^{13}C and other N atoms, and/or not uniform strain in diamond. This measured linewidth is within the predicted range of theoretical analysis.[44]

Though NV centers are atomic sized defects, the spatial resolution for wide field imaging of microwave fields using NV fluorescence is limited by the thickness of NV layer (0.9 μm for our sample), the diffraction limit of light at the emission wavelength (600–750 nm), numerical aperture of objective (0.35 in our case), and/or resolution of CCD (which is ≈300 nm for our CCD). Taking these in to account, we conclude the spatial resolution of our apparatus is submicrometer. However, by applying a gradient external magnetic field, a spatial resolution on the order of ten nanometers is possible.[45]

The temporal resolution of our NV based FM microwave detection, i.e., the maximum detectable modulating frequency f_m, is currently 56 Hz, and is limited by the readout speed of the EM-CCD (112 frames per second). Acquisition rates larger than 3000 frames per second could be achieved using a fast CMOS camera, and by reducing the spatial resolution (e.g., by binning pixels), thus pushing f_m into kHZ range. The sensitivity to frequency deviation Δf is estimated to be 2.5 kHz $Hz^{-1/2}$ for f_m = 20 Hz (more details refer to Figure S4b in the Supporting Information).

In conclusion, we demonstrated optical microscopy and spectroscopy of microwave fields using NV centers in diamond. A sensitivity of 45 nT $Hz^{-1/2}$ of microwave magnetic field amplitude (averaging over the 5 × 5 μm^2 region), dynamic range of 33 dB in microwave power, a resolution bandwidth of 460 kHz (over a range of 170 MHz, limited by the electromagnet), and 2.5 kHz $Hz^{-1/2}$ sensitivity of a single FM microwave signal detection were demonstrated. Full 3D imaging of the vector field[34] is also possible using the proposed scheme. Perhaps one of the most promising applications of our technique is in computer hardware and software security: it is well suited for monitoring activity of integrated circuit chips.[46] Furthermore, by optimizing the diamond sample and experimental configuration, the ability of NV centers to perform spectral analysis and demodulation of FM radio signal might be of interest for communication.[47,48]

Experimental Section

Diamond Sample with NV Centers: The single crystal chemical vapor deposition (CVD) grown diamond chip (Element Six) consists high purity diamond substrate (< 1 ppb N_s) on which an additional thin layer diamond is grown that is doped with N (natural abundance 99.6% ^{14}N) during the CVD synthesis process. The thickness of the layer is 0.9 um with a concentration of 10.5 ppm as determined by secondary ion mass spectroscopy. Post synthesis the sample was irradiated with 4.5 MeV electrons at a flux $\approx 2.5\times10^{14}$ $cm^{-2}s^{-1}$ for 10 h and then annealed at 800 °C for 8 h and 1200 °C for 1 h. The density of NV^- is estimated as 3–4 ppm by measuring the optical absorption at liquid nitrogen temperatures. By integrating the absorption coefficient across defect's zero-phonon-line, it can be converted into a NV concentration.[49] The CVD diamond chip is grown in the crystal direction of <100>, and the side surface of the diamond is <110>, and the NV centers are in direction of <111>.

Experimental Setup for Fluorescence Imaging of NV Centers: The detailed experimental setup is shown in Figure S1 (Supporting Information). A 532 nm probe laser (Coherent Compass 315M-100) is attenuated by neutral density filters (Thorlabs, FW2AND) to adjust the power as needed, followed by a beam expander, a convex lens, and an objective (Olympus SLMPlan 50X/0.35NA or 20X/0.35NA as needed) providing wide field illumination. The laser power is measured by a power meter (Newport 1928-C). The fluorescence of NV centers is collected by the same objective, and filtered (532-nm Semrock StopLine notch filter, E-grade, and 632.8-nm Semrock EdgeBasic long-wavelength-pass filter) before it is sent to an EM-CCD (Hamamatsu C9100-13). The optical path for fluorescence is secured inside an inverted microscope (Olympus IX71) to reduce the noise from the environment. The diamond sample with NV centers is placed on the microwave structure fabricated on a cover glass on the microscope stage. The fabrication of the microwave structure is defined by photolithography, then electron beam evaporation titanium/gold layer, and lift-off. The bias magnetic field B_0 is provided by an electromagnet (APW Co. EM075-12-222), whose applied voltage is generated by a data acquisition device (NI DAQ USB-6361) with a home-made power amplification circuit (using TI LM358 Op Amp). This setup enables us to sweep the voltage applied on the electromagnet with resolution of 1 mV, resulting in the ability to tune the resonant frequency from 2.68 to 2.87 GHz. The frequency tuning sensitivity is measured to be S = –18.12(6) MHz V^{-1} (Figure 2b), and from this we obtain the frequency resolution of 18 kHz (assuming 1 mV voltage resolution). The microwave signals are generated by two function generators (HP ESG-3000A, and Rohde & Schwarz SMC100A), with a waveform generator (Agilent 33120A) for frequency modulation. The microwave spectra measured with NV centers are compared with a radio frequency real-time spectrum analyzer (RSA, Tektronix, RSA 3303B).

Supporting Information

Supporting Information is available from the Wiley Online Library or from the author.

Acknowledgements

The authors thank Srujan Meesala, Young-Ik Sohn, Dr. Vivek Venkataraman, and Mengzhen Zhang for helpful discussions. This work was supported in part by the STC Center for Integrated Quantum Materials under NSF grant DMR-1231319 and DARPA QuASAR (Award No. HR0011-11-C-0073). Y.-F.X. was supported by the National Science Foundation of China (Grant No. 61435001). R.L. was supported by the National Fund for Fostering Talents of Basic Science (Grant No. J1103205). L.S. and R.L. did measurements and analyzed data, L.S. and M.L. wrote the manuscript with the input from all authors. M.L. supervised all experiments. R.L. and Y.-F.X. did theoretical analysis.

M.Z. helped with detection noise reduction and analysis. A.S. and X.A. helped build and optimize the setup. All authors contributed to the discussion.
Note: Ref. 16 and the Acknowledgements were corrected on July 20, 2016.

Received: January 24, 2016
Revised: March 18, 2016
Published online: May 11, 2016

[1] S. Anlage, V. Talanov, A. Schwartz, in *Scanning Probe Microscopy* (Eds: S. Kalinin, A. Gruverman), Springer, New York **2007**, p. 215.
[2] N. Yu, F. Capasso, *Nat. Mater.* **2014**, *13*, 139.
[3] D. Schurig, J. J. Mock, B. J. Justice, S. A. Cummer, J. B. Pendry, A. F. Starr, D. R. Smith, *Science* **2006**, *314*, 977.
[4] K. B. Teo, E. Minoux, L. Hudanski, F. Peauger, J.-P. Schnell, L. Gangloff, P. Legagneux, D. Dieumegard, G. A. Amaratunga, W. I. Milne, *Nature* **2005**, *437*, 968.
[5] S. Neusser, D. Grundler, *Adv. Mater.* **2009**, *21*, 2927.
[6] S. Urazhdin, V. E. Demidov, H. Ulrichs, T. Kendziorczyk, T. Kuhn, J. Leuthold, G. Wilde, S. O. Demokritov, *Nat. Nanotechnol.* **2014**, *9*, 509.
[7] S. Thiele, F. Balestro, R. Ballou, S. Klyatskaya, M. Ruben, W. Wernsdorfer, *Science* **2014**, *344*, 1135.
[8] C. Auth, C. Allen, A. Blattner, D. Bergstrom, M. Brazier, M. Bost, M. Buehler, V. Chikarmane, T. Ghani, T. Glassman, R. Grover, W. Han, D. Hanken, M. Hattendorf, P. Hentges, R. Heussner, J. Hicks, D. Ingerly, P. Jain, S. Jaloviar, R. James, D. Jones, J. Jopling, S. Joshi, C. Kenyon, H. Liu, R. McFadden, B. McIntyre, J. Neirynck, C. Parker, L. Pipes, I. Post, S. Pradhan, M. Prince, S. Ramey, T. Reynolds, J. Roesler, J. Sandford, J. Seiple, P. Smith, C. Thomas, D. Towner, T. Troeger, C. Weber, P. Yashar, K. Zawadzki, K. Mistry, in *2012 Symp. on VLSI Technology*, Widerkehr and Associates, Montgomery Village, MD, USA **2012**, p. 131.
[9] E. C. Burdette, F. L. Cain, J. Seals, *IEEE Trans. Microwave Theory Tech.* **1980**, *28*, 414.
[10] E. A. Ash, G. Nicholls, *Nature* **1972**, *237*, 510.
[11] E. Betzig, J. K. Trautman, *Science* **1992**, *257*, 189.
[12] E. Betzig, J. K. Trautman, T. D. Harris, J. S. Weiner, R. L. Kostelak, *Science* **1991**, *251*, 1468.
[13] R. C. Black, F. C. Wellstood, E. Dantsker, A. H. Miklich, D. T. Nemeth, D. Koelle, F. Ludwig, J. Clarke, *Appl. Phys. Lett.* **1995**, *66*, 99.
[14] Y. S. Greenberg, *Rev. Mod. Phys.* **1998**, *70*, 175.
[15] D. Budker, M. Romalis, *Nat. Phys.* **2007**, *3*, 227.
[16] A. Horsley, G.-X. Du, P. Treutlein, *New J. Phys.* **2015**, *17*, 112002.
[17] L. Childress, M. V. Gurudev Dutt, J. M. Taylor, A. S. Zibrov, F. Jelezko, J. Wrachtrup, P. R. Hemmer, M. D. Lukin, *Science* **2006**, *314*, 281.
[18] R. Schirhagl, K. Chang, M. Loretz, C. L. Degen, *Annu. Rev. Phys. Chem.* **2014**, *65*, 83.
[19] V. V. Dobrovitski, G. D. Fuchs, A. L. Falk, C. Santori, D. D. Awschalom, *Annu. Rev. Condens. Matter Phys.* **2013**, *4*, 23.
[20] P. Maletinsky, S. Hong, M. S. Grinolds, B. Hausmann, M. D. Lukin, R. L. Walsworth, M. Loncar, A. Yacoby, *Nat. Nanotechnol.* **2012**, *7*, 320.
[21] J. M. Taylor, P. Cappellaro, L. Childress, L. Jiang, D. Budker, P. R. Hemmer, A. Yacoby, R. Walsworth, M. D. Lukin, *Nat. Phys.* **2008**, *4*, 810.
[22] K. Arai, C. Belthangady, H. Zhang, N. Bar-Gill, S. DeVience, P. Cappellaro, A. Yacoby, R. Walsworth, *Nat. Nanotechnol.* **2015**, *10*, 859.
[23] M. Chipaux, A. Tallaire, J. Achard, S. Pezzagna, J. Meijer, V. Jacques, J.-F. Roch, T. Debuisschert, *Eur. Phys. J. D* **2015**, 69.
[24] C. L. Degen, M. Poggio, H. J. Mamin, C. T. Rettner, D. Rugar, *Proc. Natl Acad. Sci. USA* **2009**, *106*, 1313.
[25] P. Neumann, J. Beck, M. Steiner, F. Rempp, H. Fedder, P. R. Hemmer, J. Wrachtrup, F. Jelezko, *Science* **2010**, *329*, 542.
[26] H. J. Mamin, M. Kim, M. H. Sherwood, C. T. Rettner, K. Ohno, D. D. Awschalom, D. Rugar, *Science* **2013**, *339*, 557.
[27] T. Staudacher, F. Shi, S. Pezzagna, J. Meijer, J. Du, C. A. Meriles, F. Reinhard, J. Wrachtrup, *Science* **2013**, *339*, 561.
[28] A. O. Sushkov, I. Lovchinsky, N. Chisholm, R. L. Walsworth, H. Park, M. D. Lukin, *Phys. Rev. Lett.* **2014**, 113.
[29] P. Hemmer, C. Gomes, *Science* **2015**, *347*, 1072.
[30] A. Ajoy, U. Bissbort, M. D. Lukin, R. L. Walsworth, P. Cappellaro, *Phys. Rev. X* **2015**, *5*, 011001.
[31] D. R. Glenn, K. Lee, H. Park, R. Weissleder, A. Yacoby, M. D. Lukin, H. Lee, R. L. Walsworth, C. B. Connolly, *Nat. Methods* **2015**, *12*, 736.
[32] G. Kucsko, P. C. Maurer, N. Y. Yao, M. Kubo, H. J. Noh, P. K. Lo, H. Park, M. D. Lukin, *Nature* **2013**, *500*, 54.
[33] T. van der Sar, F. Casola, R. Walsworth, A. Yacoby, *Nat. Commun.* **2015**, *6*, 7886.
[34] P. Wang, Z. Yuan, P. Huang, X. Rong, M. Wang, X. Xu, C. Duan, C. Ju, F. Shi, J. Du, *Nat. Commun.* **2015**, *6*, 6631.
[35] V. Stepanov, F. H. Cho, C. Abeywardana, S. Takahashi, *Appl. Phys. Lett.* **2015**, *106*, 063111.
[36] N. Aslam, M. Pfender, R. Stohr, P. Neumann, M. Scheffler, H. Sumiya, H. Abe, S. Onoda, T. Ohshima, J. Isoya, J. Wrachtrup, *Rev. Sci. Instrum.* **2015**, *86*, 064704.
[37] P. Appel, M. Ganzhorn, E. Neu, P. Maletinsky, *New J. Phys.* **2015**, *17*, 112001.
[38] M. Chipaux, L. Toraille, C. Larat, L. Morvan, S. Pezzagna, J. Meijer, T. Debuisschert, *Appl. Phys. Lett.* **2015**, *107*, 233502.
[39] M. W. Doherty, F. Dolde, H. Fedder, F. Jelezko, J. Wrachtrup, N. B. Manson, L. C. L. Hollenberg, *Phys. Rev. B* **2012**, *85*, 205203.
[40] N. B. Manson, J. P. Harrison, M. J. Sellars, *Phys. Rev. B* **2006**, *74*, 104303.
[41] R. Lucio, B. Hannes, S. Toeno van der, H. Ronald, *New J. Phys.* **2011**, *13*, 025013.
[42] V. M. Acosta, E. Bauch, M. P. Ledbetter, A. Waxman, L. S. Bouchard, D. Budker, *Phys. Rev. Lett.* **2010**, *104*, 070801.
[43] G. C. Bjorklund, *Opt. Lett.* **1980**, *5*, 15.
[44] Z.-H. Wang, S. Takahashi, *Phys. Rev. B* **2013**, *87*, 115122.
[45] E. H. Chen, O. Gaathon, M. E. Trusheim, D. Englund, *Nano Lett.* **2013**, *13*, 2073.
[46] D. Agrawal, B. Archambeault, J. Rao, P. Rohatgi, in *Cryptographic Hardware and Embedded Systems—CHES 2002*, Vol. *2523* (Eds: B. Kaliski, Ç. Koç, C. Paar), Springer, Berlin/Heidelberg, Germany **2003**, p. 29.
[47] C.-P. Chang, H.-R. Chuang, *Electron. Lett.* **2005**, *41*, 696.
[48] R. Pabst, B. H. Walke, D. C. Schultz, P. Herhold, H. Yanikomeroglu, S. Mukherjee, H. Viswanathan, M. Lott, W. Zirwas, M. Dohler, *IEEE Commun. Mag.* **2004**, *42*, 80.
[49] G. Davies, *Phys. B: Condens. Matter* **1999**, *273-274*, 15.